

PAPER

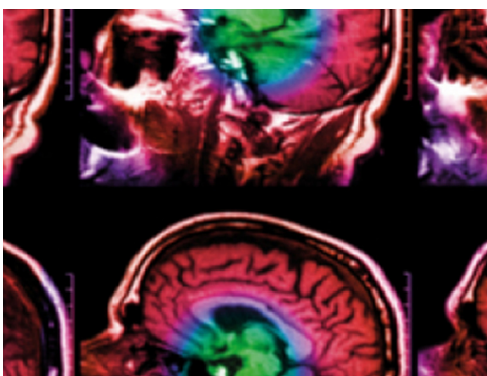
A temperature-dependent gain compensation technique for positron emission tomography detectors based on a silicon photomultiplier

To cite this article: Hyeong Seok Shim *et al* 2021 *Phys. Med. Biol.* **66** 205015

View the [article online](#) for updates and enhancements.

You may also like

- [Comparison of acrylic polymer adhesive tapes and silicone optical grease in light sharing detectors for positron emission tomography](#)
Devin J Van Elburg, Scott D Noble, Simone Hagey *et al.*
- [Primary, scatter, and penetration characterizations of parallel-hole and pinhole collimators for I-123 SPECT](#)
Arda Könik, Benjamin Auer, Jan De Beenhouwer *et al.*
- [The influence of triple energy window scatter correction on activity quantification for \$^{177}\text{Lu}\$ molecular radiotherapy](#)
Andrew P Robinson, Jill Tipping, David M Cullen *et al.*



IPEM | IOP

Series in Physics and Engineering in Medicine and Biology

Your publishing choice in medical physics,
biomedical engineering and related subjects.

Start exploring the collection—download the
first chapter of every title for free.



PAPER

A temperature-dependent gain compensation technique for positron emission tomography detectors based on a silicon photomultiplier

Hyeong Seok Shim^{1,2,3}, Haewook Park^{3,4} and Jae Sung Lee^{1,2,3,4,5} ¹ Interdisciplinary Program of Bioengineering, Seoul National University, Seoul, Republic of Korea² Integrated Major in Innovative Medical Science, Seoul National University Graduate School, Republic of Korea³ Department of Nuclear Medicine, Seoul National University College of Medicine, Seoul, Republic of Korea⁴ Department of Biomedical Sciences, Seoul National University College of Medicine, Seoul, Republic of Korea⁵ Brightonix Imaging Inc., Seoul, Republic of KoreaE-mail: jaes@snu.ac.kr**Keywords:** PET, PET detector, gain compensation, temperature, temperature sensor**Abstract**

In this study, we propose a simple gain compensation technique for silicon photomultiplier (SiPM)-based positron emission tomography detectors, using a temperature sensor that automatically controls the bias voltage of the SiPM depending upon the ambient temperature. The temperature sensor output, for which the temperature coefficient can be controlled by the input voltage, is used as one end of the bias voltage. By adjusting the temperature coefficient, the proposed gain compensation method can be applied to various SiPMs with different breakdown voltages. As a proof of concept, the proposed method was evaluated for two scintillation detector setups. Applying the proposed method to a single-channel SiPM (ASD-NUV3S-P; AdvanSiD, Italy) coupled with a 3 mm × 3 mm × 20 mm LGSO crystal, the 511 keV photopeak position in the energy histogram changed by only 1.52% per 10 °C while, without gain compensation, it changed by 13.27% per 10 °C between 10 °C and 30 °C. On a 4 × 4 array MPCC (S14161-3050HS-04; Hamamatsu, Japan), coupled with a 3.12 mm × 3.12 mm × 15 mm 4 × 4 LSO array, the photopeak changes with and without gain compensation were 2.34% and 20.53% per 10 °C between 10 °C and 30 °C, respectively. On the wider range of temperature, between 0 °C and 40 °C, the photopeak changes with and without gain compensation were 3.09% and 20.89%, respectively. The energy resolution degradation of SiPM-based scintillation detectors operating at temperatures was negligible when the proposed gain compensation method was applied.

1. Introduction

Positron emission tomography (PET) is a functional and molecular imaging system used in nuclear medicine, which detects two 511 keV gamma rays, generated by the annihilation of a positron and an electron (Cherry and Dahlbom 2006). In the scintillation detectors used for measuring gamma rays in PET, silicon photomultipliers (SiPMs) are now widely used because of their various attractive properties, such as magnetic field insensitivity, low bias voltage, and compact size (Kwon *et al* 2011, Roncali and Cherry 2011, Yamamoto *et al* 2011, Hong *et al* 2012, Yoon *et al* 2012, Ko *et al* 2016, Levin *et al* 2016, Schug *et al* 2016, Zhang *et al* 2018, Alberts *et al* 2021, Kim *et al* 2021, Won *et al* 2021). However, as the mechanism of the detector is based on avalanche breakdown, the gain of the SiPM is dependent on temperature. The mean free path for electrons decreases with increasing temperature and thus a higher electric field is required to start the avalanche process (Gundacker and Heering 2020). Therefore, a higher temperature results in a lower SiPM gain because the gain is proportional to the overvoltage, i.e. the difference between the applied bias voltage and the breakdown voltage (Lee and Hong 2010, Ko *et al* 2016).

To differentiate between the 511 keV gamma-ray events and those whose energy is lowered by Compton scattering, the energy of each event is measured by integrating the output pulse from the SiPM-based scintillation detector and plotted as an energy histogram. The peak in the histogram is called the photopeak and the position of the peak is considered as 511 keV. Events in a specific range around the photopeak are considered

to be valid 511 keV events. Owing to the temperature dependence of the SiPM gain, the estimated energy of the signals varies with changing temperature. Therefore, the energy variation caused by changing temperature results in inaccurate determination of true 511 keV events, degrading the PET image quality (Kaplan 2009).

Therefore, to maintain a constant gain regardless of the temperature change, a compensation system for the temperature dependence of the SiPM gain is required. Various gain compensation methods are proposed, using FPGA (Zhou *et al* 2020), the dark current of a blind SiPM (SiPM used as a temperature sensor by measuring the dark current) (Licciulli *et al* 2013, Licciulli and Marzocca 2015), a lookup table implemented in a microcontroller unit (Gil *et al* 2011, Ko *et al* 2016), thermometer (Miyamoto *et al* 2009), and diode (Kuznetsov 2018). The methods based on FPGA or lookup tables allow for accurate gain compensation; however, the devices are bulky, and constructing a lookup table for each detector is laborious. A gain compensation method using the property that the dark current of SiPM increases with temperature has the advantage that a device with the same operating principle is used for temperature estimation; however, this method requires additional SiPM. The methods that use a thermometer or diode exploit the linear temperature dependence of the breakdown voltage of SiPM and can be easily implemented using a small number of devices. However, both methods necessitate an additional current source and the method using diodes requires diode chains for compensation, with a different number of diodes depending on the SiPM's temperature property. The mechanism of these two methods can be interpreted as implementing a customized temperature sensor, providing an analog voltage output that changes linearly with temperature. Therefore, an off-the-shelf temperature sensor can be an alternative to temperature compensation technology with improved circuit simplicity.

In this study, we propose a novel, simple gain compensation technique for SiPM-based PET detectors using a temperature sensor that automatically controls the bias voltage of the SiPM, depending upon the ambient temperature. The output of the temperature sensor, for which the temperature coefficient can be controlled by the input voltage, is used as one end of the bias voltage. By adjusting the temperature coefficient, the proposed gain compensation method can be applied to various SiPMs with different breakdown voltages. As a proof of concept, the proposed method was evaluated with two scintillation detector setups.

2. Materials and methods

2.1. Temperature compensation technique

2.1.1. Relation between gain and temperature

The SiPM consists of single-photon avalanche diodes (SPADs), which are independent microcells (photodiode plus quenching register) working in a limited Geiger mode. As the SiPM output is the sum of the signal from each microcell fired by an incident photon, the gain of the SiPM is determined by the amount of charge flowing per avalanche (Acerbi and Gundacker 2019). To operate the microcells in Geiger mode, the operational bias voltage (V_{bias}) must be higher than the breakdown voltage (V_{bd}). The excess bias voltage over the breakdown voltage is called the overvoltage ($\Delta V = V_{bias} - V_{bd}$). The relationship between the gain of the SiPM (G) and the overvoltage (ΔV) is as follows:

$$G = \frac{C_{pixel} \times \Delta V}{e},$$

where C_{pixel} is the total capacitance of a single microcell and e is the elementary charge. Because both values are independent of temperature, if we differentiate this equation with respect to temperature, the derivative of the gain is linear to the derivative of the overvoltage. Therefore, to achieve a fixed gain of SiPM over temperature, the overvoltage must be constant regardless of the temperature. The relationship between the breakdown voltage and temperature (T) is as follows:

$$V_{bd}(T) = V_{bd,ref}(1 + \beta(T - T_{ref})),$$

where T_{ref} is the reference temperature, $V_{bd,ref}$ is the breakdown voltage measured at T_{ref} and β is the differential value of the breakdown voltage to the temperature. Because β is independent of temperature, the SiPM breakdown voltage has a linear relationship with temperature (Otte 2006, Dinu *et al* 2010). Therefore, to maintain constant overvoltage with temperature, the operational bias voltage must change linearly to the same degree as the breakdown voltage.

2.1.2. Temperature sensor

The temperature sensor used in this study was an AD22103 Analog Device (Norwood, MA, US). The temperature coefficient of the AD22103 sensor can be controlled by changing the input voltage; therefore, the sensor can be used to compensate for the temperature dependence of various detectors. The transfer function of the temperature sensor is expressed as follows

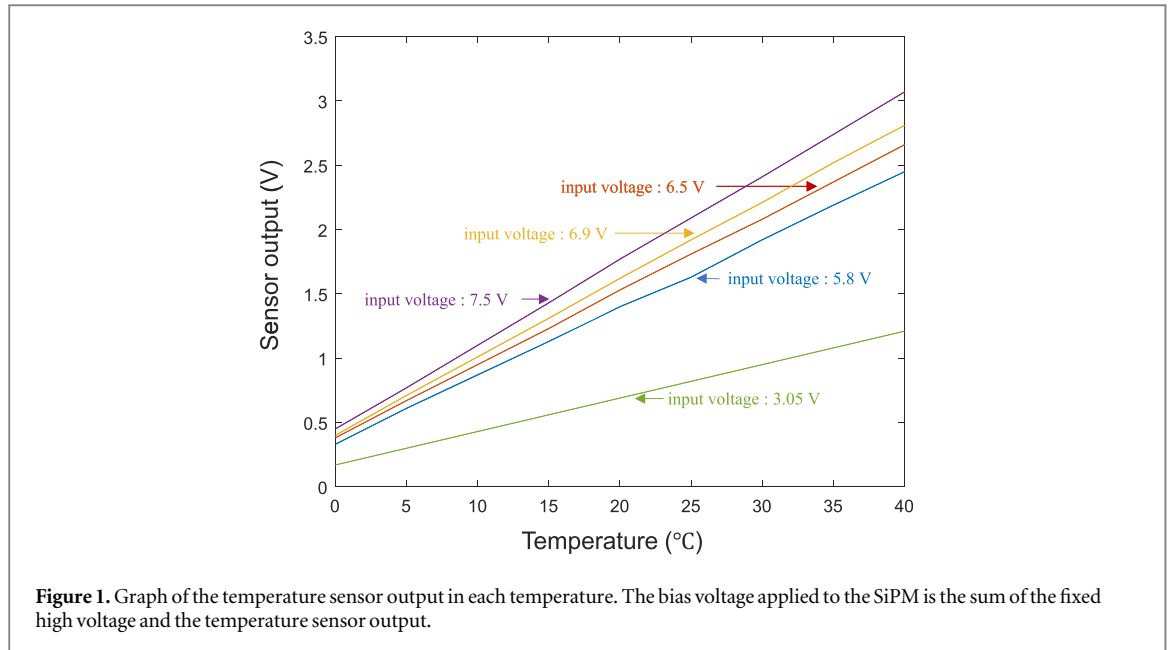


Table 1. Temperature sensor output according to temperature.

	Output voltage (V)									
	0 °C	5 °C	10 °C	15 °C	20 °C	25 °C	30 °C	35 °C	40 °C	
Input voltage (V)	3.05	0.17	0.3	0.43	0.56	0.69	0.82	0.95	1.08	1.21
	5.8	0.33	0.61	0.87	1.13	1.4	1.63	1.92	2.19	2.45
	6.5	0.38	0.67	0.95	1.23	1.53	1.81	2.08	2.37	2.66
	6.9	0.40	0.71	1.01	1.31	1.62	1.92	2.21	2.52	2.81
	7.5	0.45	0.77	1.10	1.43	1.77	2.09	2.41	2.74	3.07

$$V_{out} = (V_s/3.3 \text{ V}) \times [0.25 \text{ V} + (28 \text{ mV}/^\circ\text{C}) \times T_A],$$

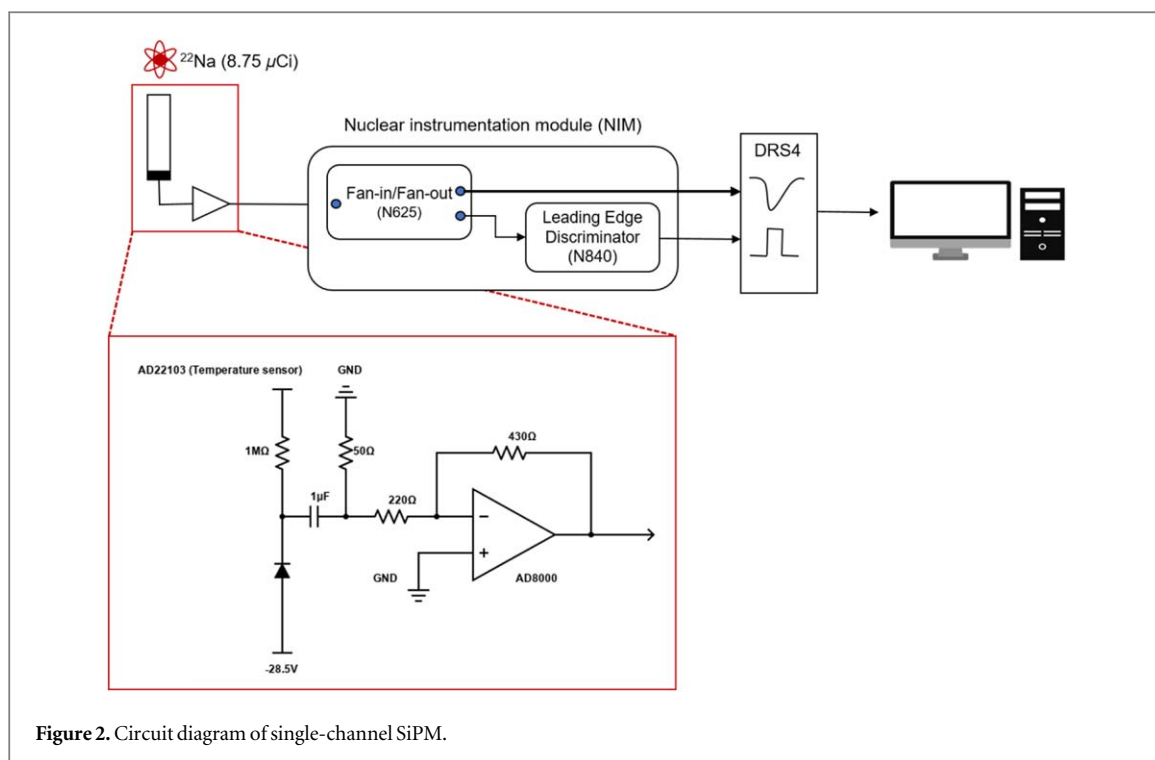
where V_s is the input voltage of the temperature sensor and T_A is the temperature ($^\circ\text{C}$).

The bias voltage was set as the sum of the temperature sensor output and a fixed high voltage to linearly change the operational bias voltage to the same degree as the breakdown voltage. The temperature coefficient of the sensor and the temperature dependence of SiPM's breakdown voltage were best matched with the smallest difference by applying an input voltage of 3.05 V for the single-channel SiPM (ASD-NUV3S-P; AdvanSiD, Italy) on the temperature range of 10 $^\circ\text{C}$ –30 $^\circ\text{C}$. The best-matched input voltage for the multi-channel 4 \times 4 SiPM (S14161-3050HS-04; Hamamatsu Photonics K.K., Hamamatsu, Japan) was 6.5 V on the temperature range of 10 $^\circ\text{C}$ –30 $^\circ\text{C}$, 5.8 V on the temperature range of 0 $^\circ\text{C}$ –30 $^\circ\text{C}$, 7.5 V on the temperature range of 10 $^\circ\text{C}$ –40 $^\circ\text{C}$, and 6.9 V on the temperature range of 0 $^\circ\text{C}$ –40 $^\circ\text{C}$. To verify the linearity of the temperature sensor, the output of the temperature sensor was monitored using an oscilloscope (DSOX3034T, 350 MHz analog bandwidth; Keysight Technologies, USA). The output of the temperature sensor with varying temperatures is presented in table 1 and shown in figure 1. As shown in figure 1, the output of the temperature sensor was linear.

The output value of the temperature sensor can match the required amount of change in SiPM bias voltage, but from a circuit design point of view, the current sinking capability of the temperature sensor is inappropriate as a voltage source. Therefore, to prevent the SiPM current from sinking to the temperature sensor, the output of the temperature sensor was connected to a 1 M Ω resistor then applied to the cathode of the SiPM. The node after the DC cut capacitance was grounded with 50 Ω resistance to convert SiPM current to voltage.

2.2. Detector and data acquisition setup

To verify the proposed method, we used two detector setups: a 3 mm \times 3 mm pitch single-channel SiPM coupled with a 3 \times 3 \times 20 mm³ LGSO crystal and a 4 \times 4 SiPM with each channel of 3 mm \times 3 mm pitch coupled with a 4 \times 4 array of 3.12 \times 3.12 \times 15 mm³ LSO crystal. Crystals are all wrapped with ESR film. The SiPM and crystal were coupled using BC-630 optical grease (Saint-Gobain S.A., Courbevoie, France) and a ²²Na point source (8.75 μCi) was used for irradiation with gamma rays. The detector setups were placed in a thermostatic chamber to control the temperature. Because the single-channel SiPM setup was evaluated to show the initial feasibility of the proposed method, the temperature range was only from 10 $^\circ\text{C}$ to 30 $^\circ\text{C}$. The



multi-channel SiPM setup was evaluated to verify the feasibility and system-level applicability of the proposed method. Therefore, experiments were conducted in various temperature ranges: 10 °C–30 °C, 10 °C–40 °C, 0 °C–30 °C, and 0 °C–40 °C. The results were compared with the non-compensation condition, in which the bias voltage was fixed to be 1.5 V higher than the high voltage used in the compensation condition as the output of the temperature sensor on 20 °C is about 1.5 V.

2.2.1. Single-channel SiPM

The breakdown voltage of the single-channel SiPM ASD-NUV3S-P was 26.5 V at room temperature (20 °C). For the bias voltage supply to the SiPM, the SiPM cathode was connected directly to the output terminal of the temperature sensor via a 1 MΩ resistor while the SiPM anode was connected to a fixed voltage of –28.5 V (figure 2). After passing through an inverting amplifier, the output from the SiPM cathode was connected to the nuclear instrument modules (NIMs) fan-in/fan-out module (N625; CAEN S.p.A, Viareggio, Italy) and branched in two ways: one to the waveform digitizer (DT 5742 B; CAEN), based on the domino-ring-sampler 4, and the other to the leading edge discriminator module (N840; CAEN), to generate a trigger signal (figure 2). The trigger signal was then provided to the DT 5742 B.

2.2.2. 4 × 4 SiPM array

The breakdown voltage of the 4 × 4 SiPM array S14161-3050HS-04 was 38.21 V at room temperature (20 °C). For the bias voltage supply to the SiPM, the cathodes of 16 SiPM channels were merged through a 1 MΩ resistor and connected to the output terminal of the temperature sensor while the SiPM anodes were merged and connected with a fixed voltage of –40 V (figure 3). The SiPM merged anode output was fed to a comparator (ADCMP601; Analog Devices, Norwood, MA, US) to generate a trigger signal. The threshold voltage supplied to the other side of the comparator was 73.90 mV. The trigger signal and output of each SiPM cathode were sent to a DT 5742 B waveform digitizer (figure 3).

2.3. Saturation correction

SiPM has a finite number of SPADs and, thus, the saturation effect occurs when the number of photons emitted from the scintillator exceeds that the SiPM can accommodate. If the saturation effect occurs, the amplitude of the SiPM output signal is not linearly proportional to the number of incident photons entering the SiPM.

Therefore, to accurately measure the exact gain of the SiPM, the saturation effect must be corrected (Kang *et al* 2015). In this study, ¹³³Ba (356 keV) and ²²Na (511 keV and 1.274 MeV) point sources were used for the saturation correction. The photopeak values of each radioisotope were measured using an energy histogram. The relationship between the measured value and known energy of the photopeak was fitted to the equation below to determine the saturation effect of the SiPM

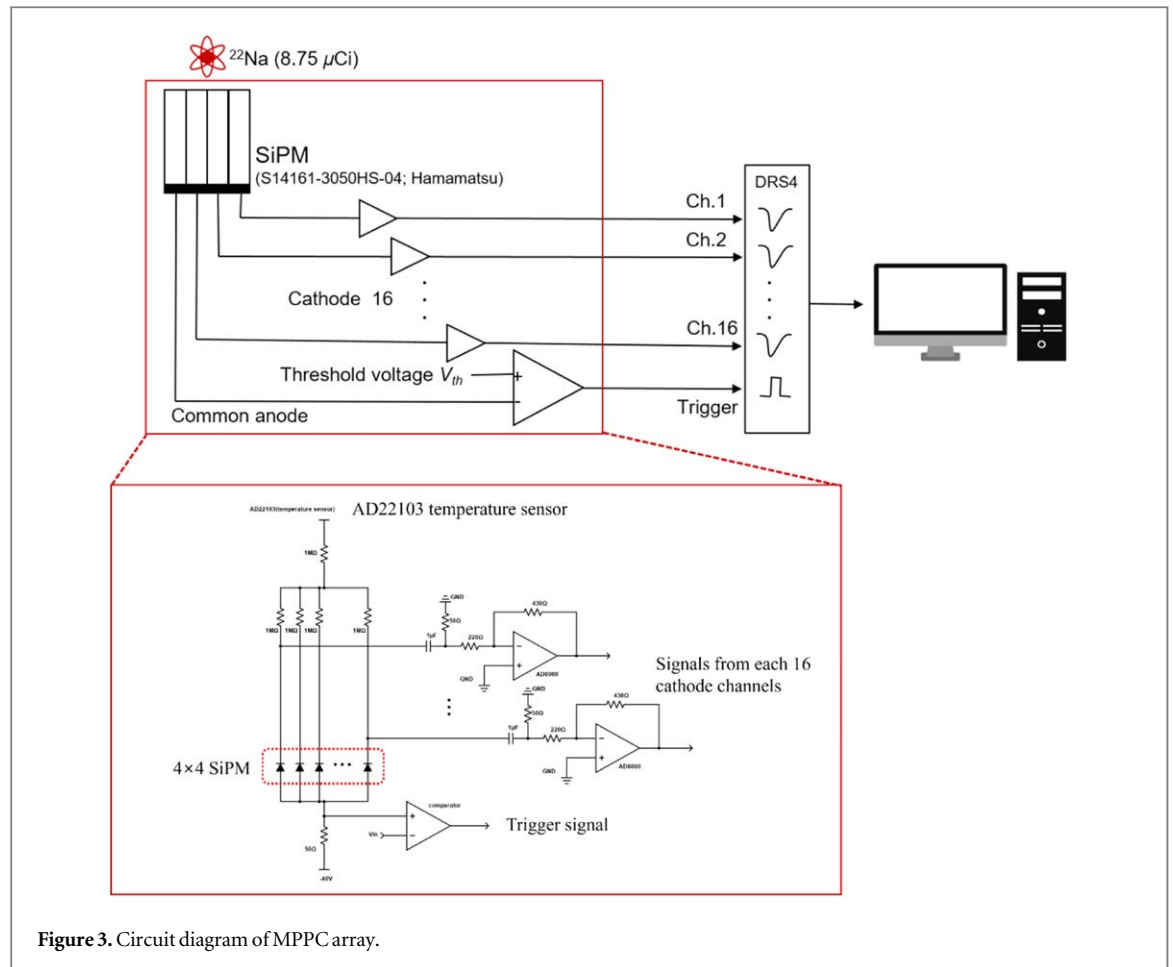


Figure 3. Circuit diagram of MPPC array.

$$y = a(1 - e^{-bx}),$$

where y is the measured photopeak value on the energy histogram, x is the known energy of the photopeak, and a and b are constants to be determined. The tangent line at the origin of the curve allows the photopeak value to be estimated when no saturation effect has occurred. To correct for the saturation effect, the ratio of the 511 keV value on the curve to the value on the tangent line was multiplied by the SiPM's output amplitude. In this study, all gains were corrected for the saturation effects.

3. Results

3.1. Single-channel SiPM

3.1.1. Optimal input voltage of temperature sensor

To find the optimal input voltage of the temperature sensor to compensate for the gain drift of the SiPM with temperature change, the peak positions were measured at various temperatures, i.e. from 10 °C to 30 °C at 2 °C intervals. As the temperature dependence of the single-channel SiPM ASD-NUV3S-P is 26 mV °C⁻¹ as indicated in the datasheet, we solved the following equation and got the calculated optimal input voltage as 3.06 V.

$$(V_s/3.3 \text{ V}) \times (28 \text{ mV}/^\circ\text{C}) = 26 \text{ mV}/^\circ\text{C}.$$

The tested input voltage of the temperature sensor was 3.0, 3.05, 3.1 V with the same single-channel SiPM ASD-NUV3S-P. The difference of the temperature coefficient of input voltage 3.05 and 3.06 V was less than 1 mV which is within the margin of error. For the convenience of setting, the experiment was conducted with the input voltage in units of 50 mV. As presented in table 2 and figure 4, when 3.05 V was applied, the gain drift of the SiPM over the temperature change was best compensated and the peak position variation was 1.52% per 10 °C, relative to the value at 20 °C. The energy resolution was also consistent (12.17%, ±0.53%).

3.1.2. Error rate with a fixed energy window

Figure 5 shows the energy histograms measured at 10 °C, 15 °C, 25 °C, and 30 °C while compensating for the SiPM gain drift using the proposed method. The error rates of counting valid 511 keV events are summarized in table 3. To calculate the error rates, a ±10% energy window around the 511 keV peak obtained at 20 °C was

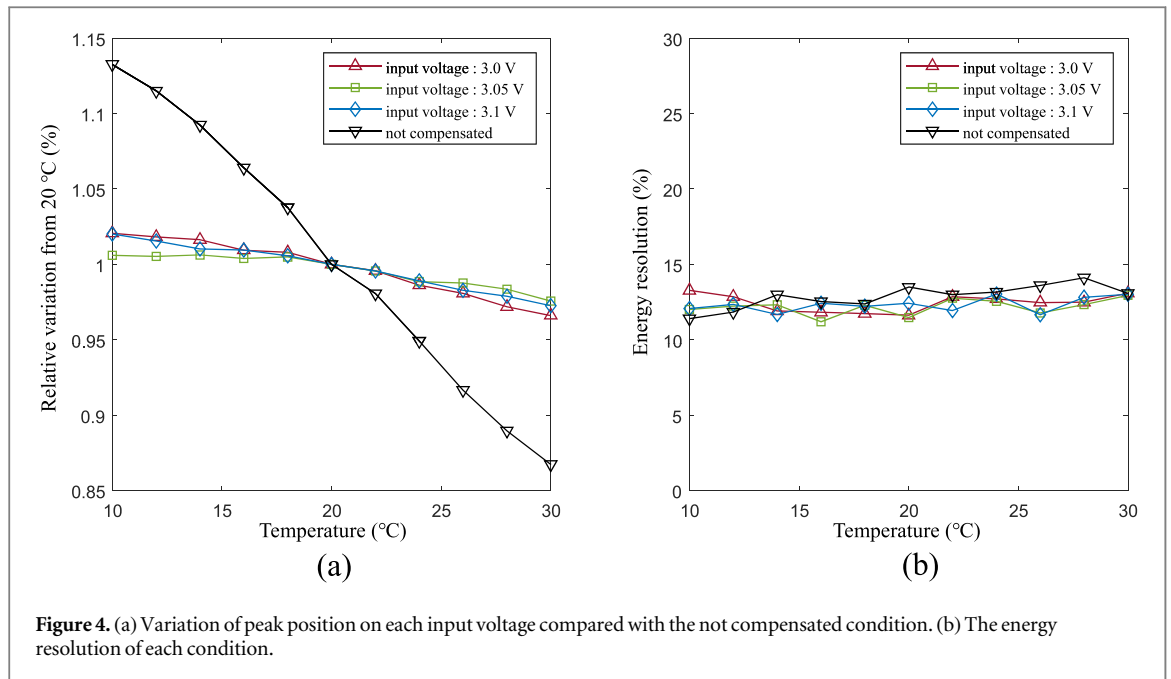


Figure 4. (a) Variation of peak position on each input voltage compared with the not compensated condition. (b) The energy resolution of each condition.

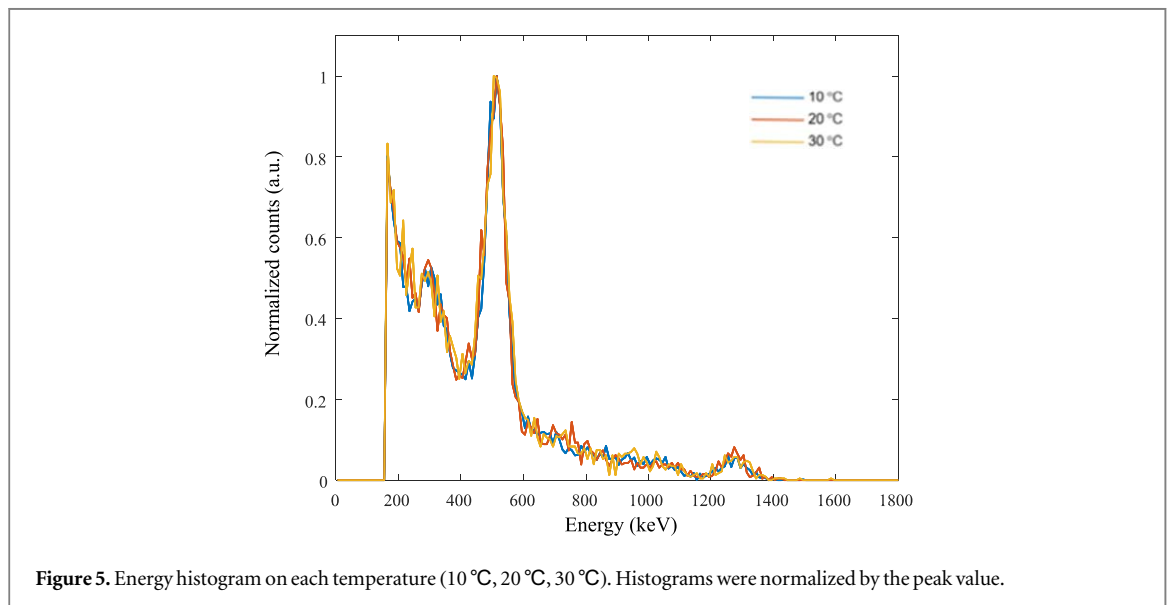


Figure 5. Energy histogram on each temperature (10 °C, 20 °C, 30 °C). Histograms were normalized by the peak value.

Table 2. Peak position variation and energy resolution according to the input voltage of the temperature sensor.

Input voltage (V)	Peak position variation (%/10 °C)	Energy resolution (%)
3.0	3.39	12.44 ± 0.58
3.05	1.52	12.17 ± 0.53
3.1	2.74	12.33 ± 0.48
No compensation	13.27	12.87 ± 0.79

applied to other energy histograms measured at 10 °C, 15 °C, 25 °C, and 30 °C and the number of events in the energy window was counted.

3.1.3. Energy resolution during temperature change

For an input voltage of 3.05 V, the energy resolution was measured during a temperature change from 10 °C to 30 °C. The measured energy spectra and energy resolutions were compared with and without the applied compensation technique (figure 6 and table 4). As summarized in table 4, without compensation, the energy

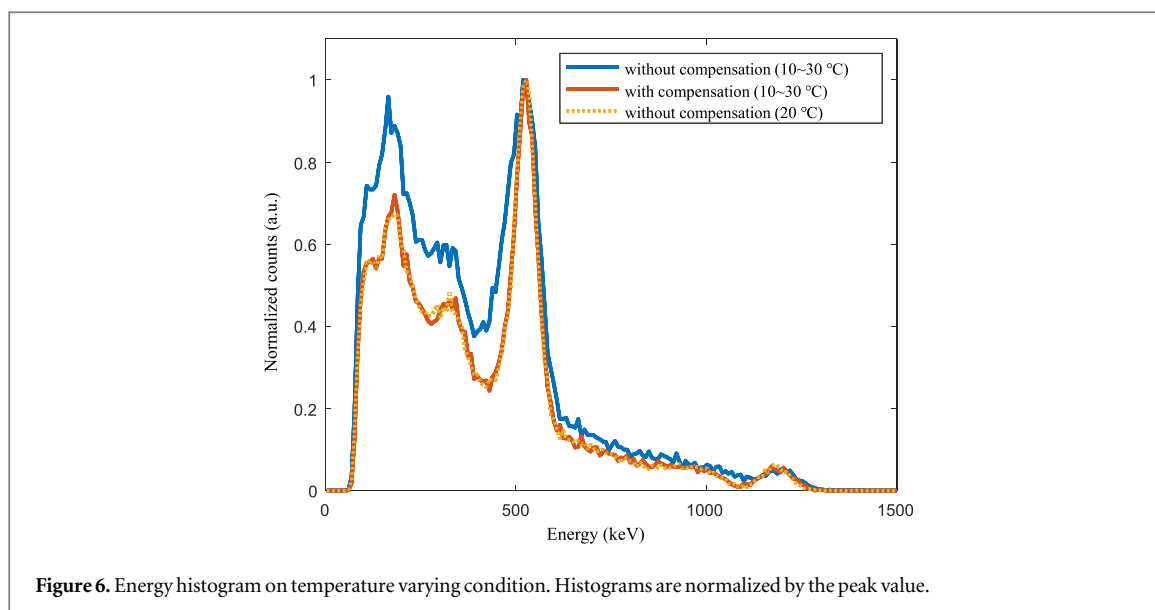


Figure 6. Energy histogram on temperature varying condition. Histograms are normalized by the peak value.

Table 3. Count rate error occurred when applying $\pm 10\%$ energy window around 511 keV peak obtained at 20 °C to other energy histograms measured at different temperatures using single-channel SiPM. The error rate is a value of the ratio.

	10 °C	15 °C	25 °C	30 °C
Error rate	<0.01	<0.01	0.02	0.05

Table 4. Energy resolution during temperature change.

Condition	Energy resolution (%)
Without compensation (10 °C–30 °C)	18.51
With compensation (10 °C –30 °C)	12.32
Without compensation (20 °C)	11.85

resolution was significantly degraded (18.51%); however, the SiPM gain compensation technique only slightly degraded the energy resolution.

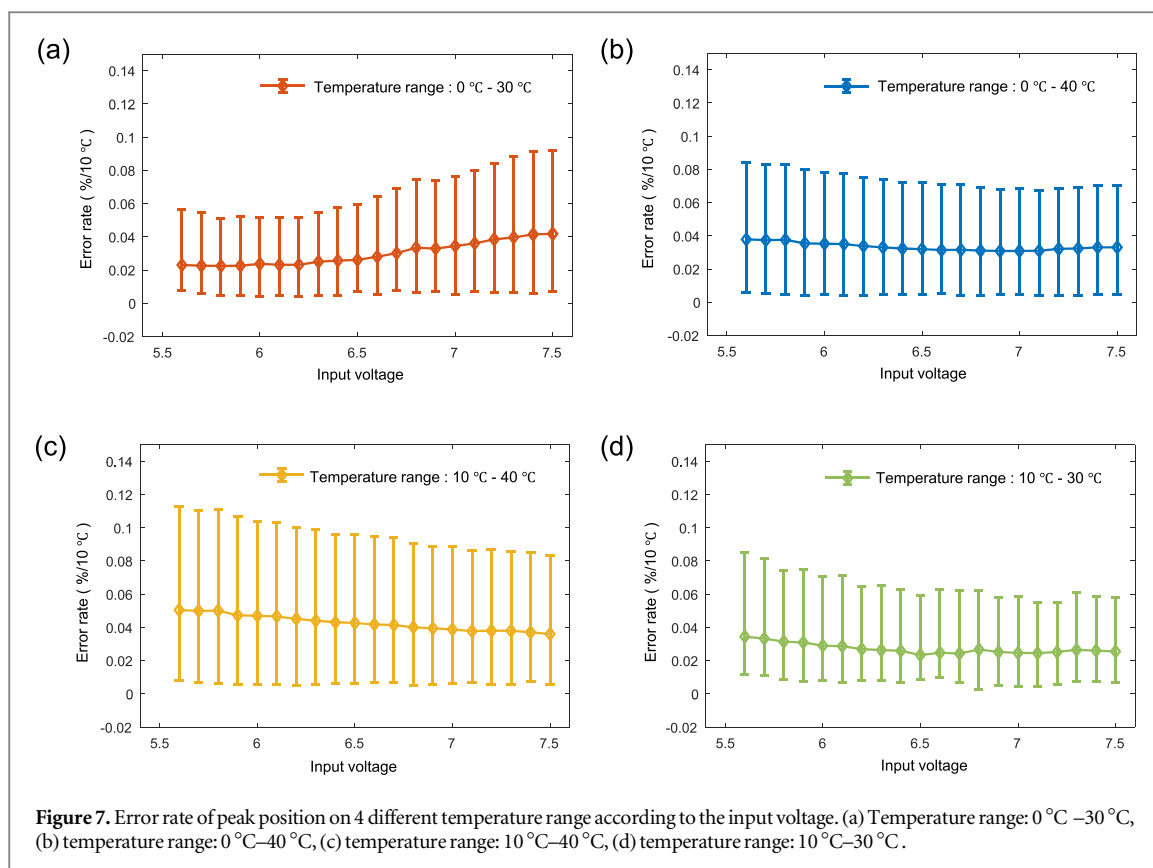
3.2. 4 × 4 SiPM array

3.2.1. Optimal input voltage of temperature sensor

The same procedure was performed using the 4 × 4 SiPM array S14161-3050HS-04. All 16 channels had the same bias voltage, temperature output voltage minus fixed high voltage. Signals from each 16 cathode channels were individually readout to measure the variation of peak position and energy resolution. We evaluated the proposed method on various conditions, the input voltage of the temperature sensor ranging from 5.6 to 7.5 V in 0.1 V intervals on 4 different temperature ranges, 10 °C–30 °C, 10 °C–40 °C, 0 °C–30 °C, and 0 °C–40 °C. As shown in figure 7, the optimal input voltage for the 4 × 4 SiPM array on 10 °C–30 °C was 6.5 V, 7.5 V on 10 °C–40 °C, 5.8 V on 0 °C–0 °C, and 6.9 V on 0 °C–40 °C. Peak position variation in energy spectrum is summarized in figure 8 and table 5.

3.2.2. Error rate with a fixed energy window

The count rate errors that occurred when applying a $\pm 10\%$ energy window around the 511 keV peak obtained at 30 °C to other energy histograms measured at different temperatures are summarized in table 6.



3.2.3. Energy resolution during temperature change

With each optimal input voltage of the temperature sensor on 4 different temperature ranges, we measured the energy resolution of each channel under the condition that the temperature changes from the lower to the upper limit of each range. As summarized in figure 9, with the proposed compensation technique, the average energy resolution for each of the 4 different temperature ranges was 11.55%, 12.65%, 12.41%, 12.11%, respectively. Without the proposed compensation technique, photopeak did not appear in several channels. In figure 9(b), black and white colors indicate the channels in which photopeak did not appear.

4. Discussions

4.1. Variation of peak position on the wider range of temperature

It is known that the SiPM breakdown voltage as a function of temperature is linear, however, it is not linear over a wide range, as shown in (figure 8(b)). With the fixed bias voltage, the peak position variation was $17.17\% \pm 1.00\%$ per $10\text{ }^{\circ}\text{C}$ on the temperature range of $0\text{ }^{\circ}\text{C}$ – $20\text{ }^{\circ}\text{C}$, and $24.61\% \pm 0.65\%$ per $10\text{ }^{\circ}\text{C}$ on the temperature range of $20\text{ }^{\circ}\text{C}$ – $40\text{ }^{\circ}\text{C}$. This shows that the gain drift of the SiPM with temperature is not linear with temperature on a wide range of temperatures. As shown in figure 10, the parabolic model fits better than the linear model for the peak positions measured without applying the compensation technique. The reason that the optimal input voltage of the temperature sensor differs for different temperature ranges would be due to the nonlinearity of the SiPM gain drift with temperature. Because of the small second-order coefficient, the gain drift of SiPM with temperature can be assumed to be linear over a narrow temperature range. However, as the temperature range is extended, the nonlinearity of the SiPM gain drift with temperature should be considered and active temperature management is recommended.

4.2. Gain compensation technique for multi-channel SiPM

Array-type SiPMs were fabricated by combining different SiPMs, which could result in differences arising in the characteristics of each channel. Also, although the temperature sensor was placed right next to the SiPM, there was a slight difference in the distance between the sensor and each channel. The SiPM channel closest to the temperature sensor was 0.5 cm away and the SiPM channel farthest was 1.4 cm away. Therefore, to use the array-type SiPM, it is necessary to verify the gain compensation method with array-type SiPM. Gain compensation methods using FPGA and lookup tables have been verified with multi-channel SiPMs by several groups and are used in actual PET systems (Gil *et al* 2011, Ko *et al* 2016). However, to the best of our knowledge, no validation

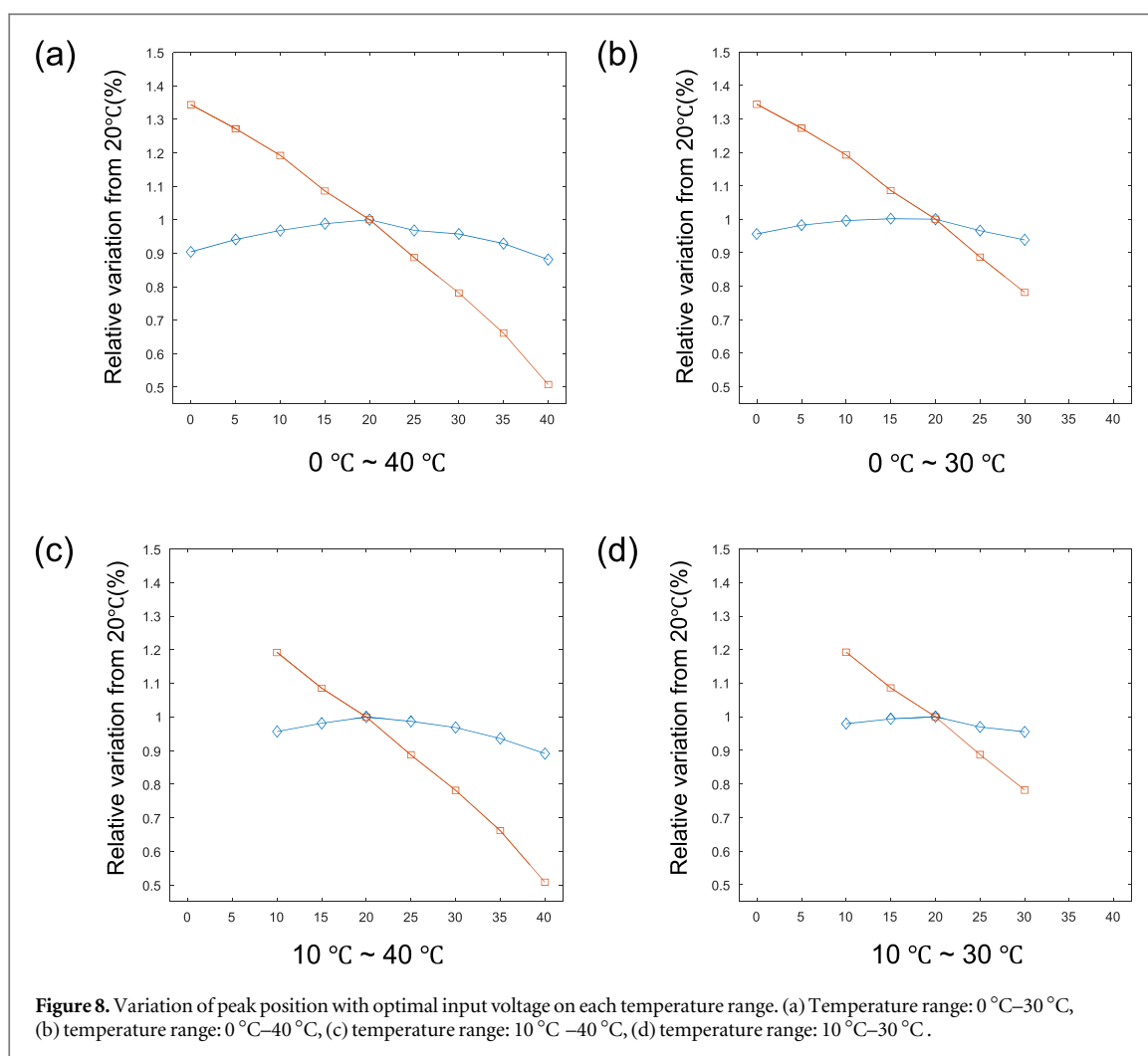


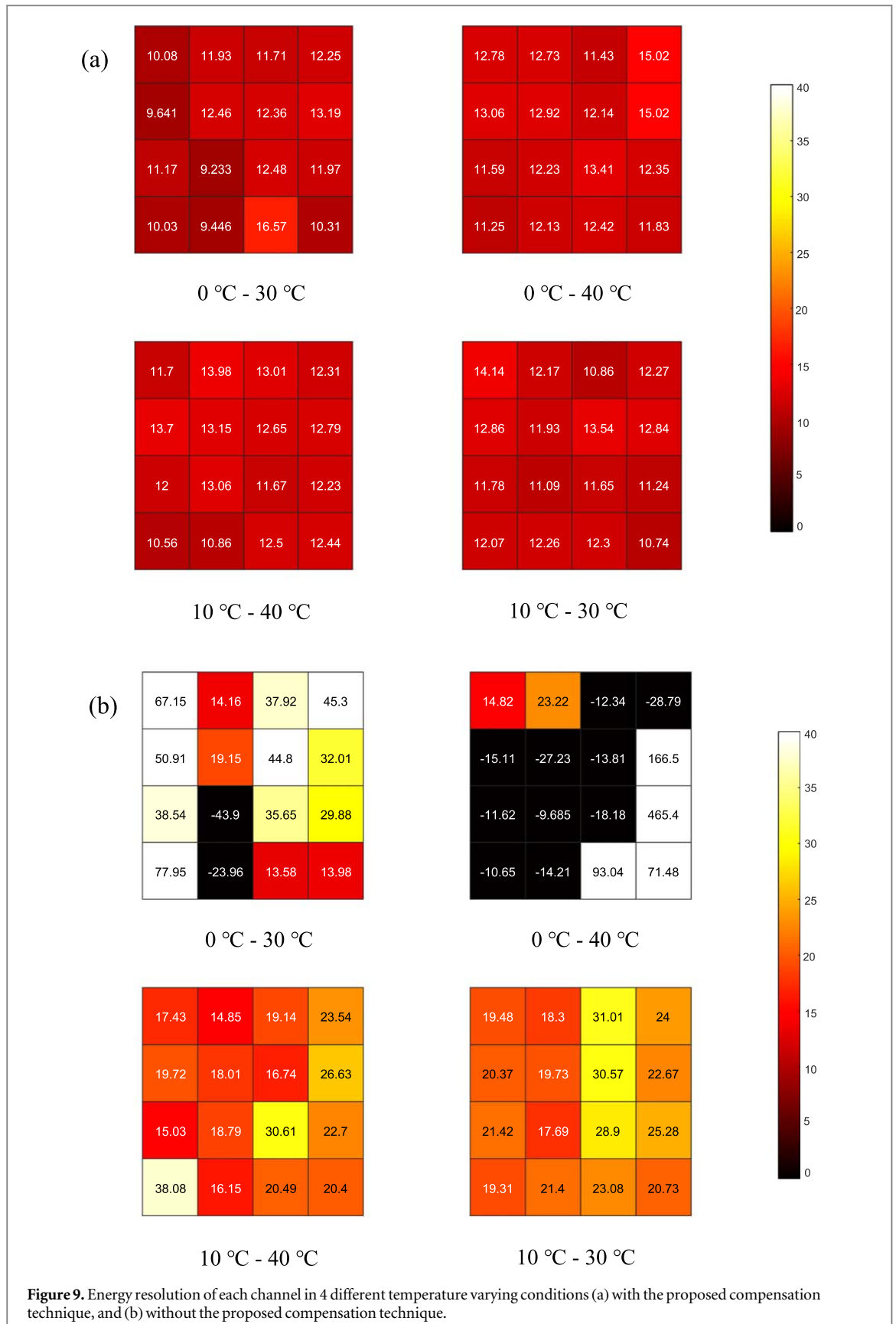
Table 5. Error rate on each temperature range with optimal input voltage and without compensation technique.

Temperature range	Optimal input voltage (V)	Error rate (% / 10 °C)	Error rate without gain compensation (% / 10 °C)
0 °C– 30 °C	5.8	2.29 ± 0.70	18.74 ± 0.86
0 °C–40 °C	6.9	3.09 ± 0.23	20.89 ± 0.78
10 °C–40 °C	7.5	3.61 ± 0.46	22.80 ± 0.85
10 °C–30 °C	6.5	2.34 ± 0.31	20.53 ± 1.01

Table 6. Count rate error occurred when applying ±10% energy window around 511 keV peak obtained at 30 °C to other energy histograms measured at different temperatures using 4 × 4 SiPM array.

Input voltage	0 °C	5 °C	10 °C	15 °C	20 °C	25 °C	35 °C	40 °C
5.8 V	0.02	0.10	0.19	0.21	0.19	0.04	0.08	0.50
6.5 V	0.11	0.11	0.03	0.05	0.06	0.02	0.17	0.41
6.9 V	0.12	0.03	0.02	0.05	0.07	0.02	0.05	0.23
7.5 V	0.65	0.10	0.02	0.02	0.05	0.02	0.06	0.25
No compensation	~1	~1	~1	~1	~1	0.62	0.70	~1

studies have been conducted on methods using blind SiPMs (Licciulli *et al* 2013, Licciulli and Marzocca 2015), thermometers (Miyamoto *et al* 2009), or diode chains (Kuznetsov 2018) for multi-channel SiPMs. The results for the 4 × 4 SiPM array obtained in this study demonstrate the potential of the proposed gain compensation method for use in real PET systems. As shown in figure 11, the photopeaks of each channel are different. After normalizing all channels to the photopeak position of (1, 1) channel, the channel with the lowest photopeak bias



was (4, 4) channel with 98.09% and that with the highest photopeak was (4, 1) channel with 110.8%. The photopeak bias of each pixel may be different because of various reasons, such as the variations in scintillation crystal light yield and optical coupling efficiency, but the breakdown voltage and the bias voltage of each channel were the same, so the gain over temperature was the same for each channel. This is because the gain drift according to the temperature of each pixel is a function of overvoltage, not photopeak bias.

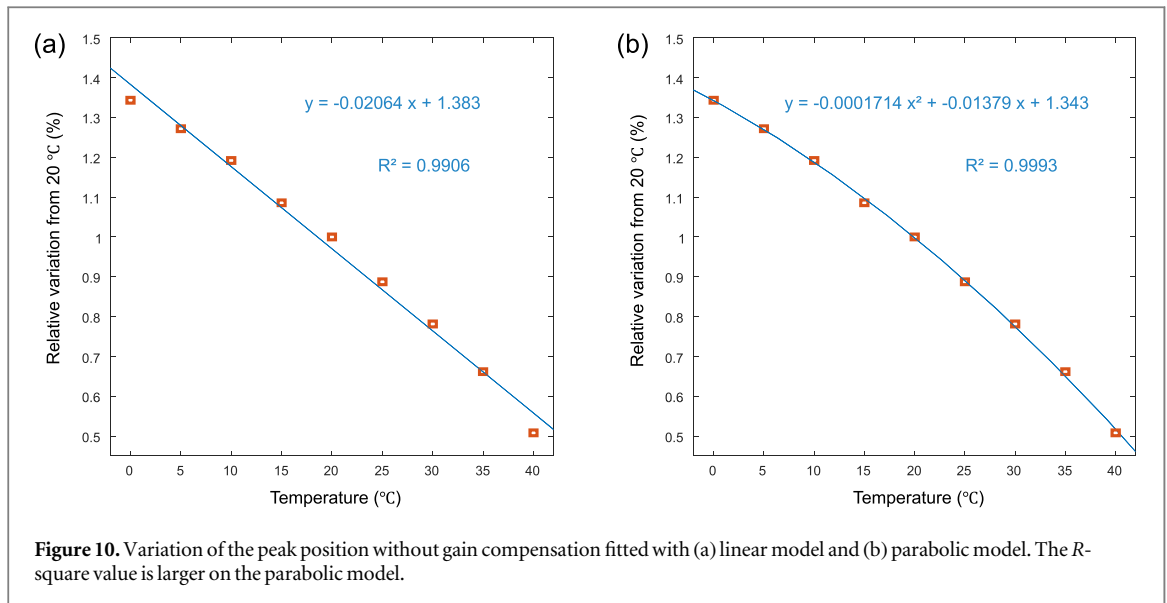


Figure 10. Variation of the peak position without gain compensation fitted with (a) linear model and (b) parabolic model. The R -square value is larger on the parabolic model.

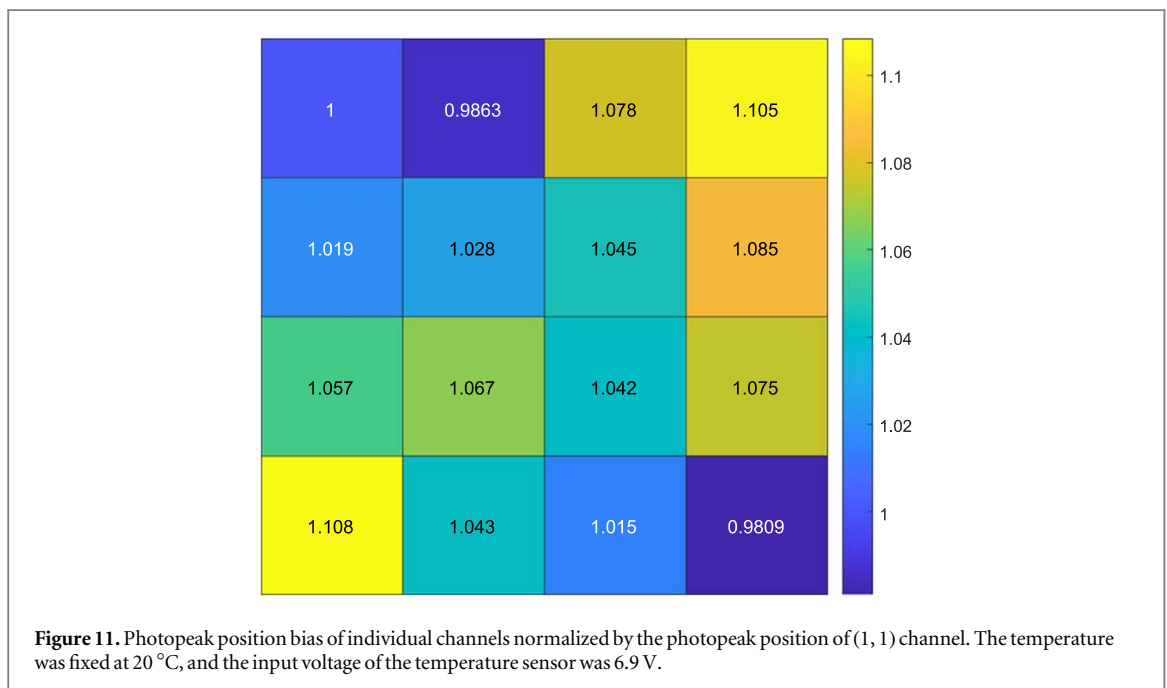


Figure 11. Photopeak position bias of individual channels normalized by the photopeak position of (1, 1) channel. The temperature was fixed at 20 °C, and the input voltage of the temperature sensor was 6.9 V.

4.3. Factors causing errors in gain compensation

4.3.1. Output variation of temperature sensor

The analog output of the temperature sensor was subjected to electronic noise. When monitoring the temperature sensor output with an oscilloscope, the signal fluctuated up to 80 mV. At a 3.3 V overvoltage of the single-channel SiPM, the 80 mV fluctuation can cause the SiPM gain to change by 2.4%. Therefore, techniques that reduce the electronic noise generated at the temperature sensor output can improve the proposed gain compensation method.

4.3.2. Heating of operational amplifier

For the 4×4 multi-channel SiPM experiments, 17 operational amplifiers were mounted on a printed circuit board (PCB). Although all experiments were performed in a thermostatic chamber, the PCB was heated by the operational amplifiers and the output of the temperature sensor attached to the PCB increased by 100 mV. For the 3.3 V overvoltage condition of the 4×4 multi-channel SiPM, the 100 mV fluctuation can cause the SiPM gain to change by more than 3%. This may explain why the proposed technique yielded higher errors in the 4×4 multi-channel SiPM than in the single-channel SiPM. Therefore, sufficient time was required to stabilize the PCB temperature to obtain equilibrium with the temperature of the thermostatic chamber. At high temperatures, the time taken to reach thermal equilibrium increases, resulting in a higher compensation error.

5. Conclusion

In this study, a simple gain compensation technique using only a temperature sensor was proposed to overcome the temperature dependence of the SiPM gain. Using the proposed technique, we compensated for the gain variation with an error of 1.52% per 10 °C in a single-channel SiPM ASD-NUV3S-P and $2.34 \pm 0.31\%$ per 10 °C in a multi-channel SiPM S14161-3050HS-04 between 10 °C and 30 °C. On the wider range of temperature, between 0 °C and 40 °C, the error of the gain variation in a multi-channel SiPM S14161-3050HS-04 slightly increased to $3.09 \pm 0.23\%$ per 10 °C. Because the implementation is simple and the performance is reasonable, this method will be useful for radiation detection and imaging.

Acknowledgments

This work was supported by grants from the National Research Foundation of Korea (NRF) funded by the Korean Ministry of Science and ICT (Grant No. 2020M2D9A1093989).

ORCID iDs

Jae Sung Lee  <https://orcid.org/0000-0001-7623-053X>

References

- Alberts I et al 2021 Clinical performance of long axial field of view PET/CT: a head-to-head intra-individual comparison of the biograph vision quadra with the biograph vision PET/CT *Eur. J. Nucl. Med. Mol. Imaging* **48** 2395–404
- Acerbi F and Gundacker S 2019 Understanding and simulating SiPMs *Nucl. Instrum. Methods Phys. Res. A* **926** 16–35
- Cherry S R and Dahlbom M 2006 *PET: Physics, Instrumentation, and Scanners* (Berlin: Springer)
- Dinu N et al 2010 Temperature and bias voltage dependence of the MPPC detectors *IEEE Nuclear Science Symposium & Medical Imaging Conf.* (Piscataway, NJ: IEEE)
- Gil A et al 2011 Programmable power supply system for SiPM bias *2011 IEEE Nuclear Science Symp. Conf. Record* (Piscataway, NJ: IEEE)
- Gundacker S and Heering A 2020 The silicon photomultiplier: fundamentals and applications of a modern solid-state photon detector *Phys. Med. Biol.* **65** 17TR01
- Hong S J et al 2012 SiPM-PET with a short optical fiber bundle for simultaneous PET-MR imaging *Phys. Med. Biol.* **57** 3869
- Kang H G et al 2015 A dual-ended readout detector using a meantime method for SiPM TOF-DOI PET *IEEE Trans. Nucl. Sci.* **62** 1935–43
- Kaplan A and C. Collaboration 2009 Correction of SiPM temperature dependencies *Nucl. Instrum. Methods Phys. Res. A* **610** 114–7
- Kim K Y et al 2021 Performance evaluation of SimPET-X, a PET insert for simultaneous mouse total-body PET/MR imaging *Mol. Imaging Biol.* **23** 703–13
- Ko G B et al 2016 Evaluation of a silicon photomultiplier PET insert for simultaneous PET and MR imaging *Med. Phys.* **43** 72–83
- Kwon S I et al 2011 Development of small-animal PET prototype using silicon photomultiplier (SiPM): initial results of phantom and animal imaging studies *J. Nucl. Med.* **52** 572–9
- Kuznetsov E 2018 Temperature-compensated silicon photomultiplier *Nucl. Instrum. Methods Phys. Res. A* **912** 226–30
- Lee J S and Hong S J 2010 Geiger-mode avalanche photodiodes for PET/MRI *Electronics for Radiation Detection* (Boca Raton, FL: CRC Press) pp 179–98
- Levin C S et al 2016 Design features and mutual compatibility studies of the time-of-flight PET capable GE SIGNA PET/MR system *IEEE Trans. Med. Imaging* **35** 1907–14
- Licciulli F et al 2013 A novel technique for the stabilization of SiPM gain against temperature variations *IEEE Trans. Nucl. Sci.* **60** 606–11
- Licciulli F and Marzocca C 2015 An active compensation system for the temperature dependence of SiPM gain *IEEE Trans. Nucl. Sci.* **62** 228–35
- Miyamoto H et al 2009 SiPM development and application for astroparticle physics experiments *31th Int. Cosmic Ray Conf. (Łódź, Poland)*
- Otte N 2006 The silicon photomultiplier—a new device for high energy physics, astroparticle physics, industrial and medical applications *Proc. 9th Int. Symp. on Detectors for Particle, Astroparticle and Synchrotron Radiation Experiments*
- Roncali E and Cherry S R 2011 Application of silicon photomultipliers to positron emission tomography *Ann. Biomed. Eng.* **39** 1358–77
- Schug D et al 2016 Initial PET performance evaluation of a preclinical insert for PET/MRI with digital SiPM technology *Phys. Med. Biol.* **61** 2851
- Won J Y et al 2021 Development and initial results of a brain PET insert for simultaneous 7-Tesla PET/MRI using an FPGA-only signal digitization method *IEEE Trans. Med. Imaging* **40** 1579–90
- Yamamoto S et al 2011 Simultaneous imaging using Si-PM-based PET and MRI for development of an integrated PET/MRI system *Phys. Med. Biol.* **57** N1
- Yoon H S et al 2012 Initial results of simultaneous PET/MRI experiments with an MRI-compatible silicon photomultiplier PET scanner *J. Nucl. Med.* **53** 608–14
- Zhang J et al 2018 Performance evaluation of the next generation solid-state digital photon counting PET/CT system *Eur. J. Nucl. Med. Mol. Imaging Res.* **8** 1–16
- Zhou A et al 2020 Study on the FPGA-based temperature compensation for the SiPM of CEPC ECAL prototype *J. Instrum.* **15** C10008